Polymer 55 (2014) 2716–2724

Contents lists available at ScienceDirect

Polymer

journal homepage: www.elsevier.com/locate/polymer

Raft crystals of poly(isoprene)-*block*-poly(ferrocenyldimethylsilane) and their surface wetting behavior during melting as observed by AFM and NanoTA

Joost Duvigneau [a], Edit Kutnyanszky [a], In Yee Phang [a], Hong-Jing Chung [a], Hairong Wu [a], Lionel Dos Ramos [a], Torben Gädt [b], Siti Fairus M. Yusoff [b,1], Mark A. Hempenius [a], Ian Manners [b], G. Julius Vancso [a,*]

[a] *Materials Science and Technology of Polymers, Mesa+ Institute for Nanotechnology, University of Twente, P.O. Box 217, 7500AE Enschede, The Netherlands*
[b] *School of Chemistry, University of Bristol, Bristol BS8 1TS, UK*

ARTICLE INFO

Article history:
Received 4 November 2013
Received in revised form
19 February 2014
Accepted 14 April 2014
Available online 24 April 2014

Keywords:
Polymer crystals
Macromolecular nanostructures
Surface wetting and melting

ABSTRACT

We report on the morphology evolution during heating and melting of lamellar poly(isoprene)-*block*-poly(ferrocenyldimethylsilane) (PI_{76}-*b*-$PFDMS_{76}$) raft crystals deposited at the native oxide surface of silicon (SiO_2) or at a highly ordered pyrolytic graphite (HOPG) surface, studied by *in situ* temperature controlled atomic force microscopy. Crystals deposited on hydrophilic SiO_2 surfaces revealed an irreversible decrease in length at temperatures of up to tens of degrees above their expected melting temperature, while maintaining their platelet-like structure. Crystals deposited on hydrophobic HOPG surfaces initially decreased in length below their expected melting temperature, while at 120 °C and above a typical molten morphology was observed. In addition, the irreversible formation of a PI_{76}-*b*-$PFDMS_{76}$ wetting layer around the crystals was observed upon increasing the temperature. These observations in the morphological behavior upon heating emphasize the role of interfacial energy between a surface deposited block copolymer based macromolecular nanostructure and its supporting substrate.

1. Introduction

The self-assembly of amphiphilic block copolymers (BCP) into well defined nanometer sized aggregates with a distinctive core–shell morphology in block-selective solvents has attracted extensive interest in recent years. In particular, the wide diversity available in architecture, shape, size, functionality and composition makes these self-organized structures attractive for utilization in *e.g.* drug delivery [1–4], catalysis [5–8] and nanolithography applications [9–11].

The functionality and properties of both the corona and core of the self-assembled BCP structures can readily be adjusted by modifying the composition of their constituent BCP chains. Poly(ferrocenyldimethylsilane) (PFDMS) based BCP assemblies prepared in a selective solvent for the non-PFDMS block have been reported in the literature and comprise an interesting class of architectures [12–15]. Due to the presence of both Fe(II) and Si in the organometallic polymer main chain, PFDMS possesses appealing properties in terms of redox activity [16–18] and etch resistance [19,20]. Furthermore, PFDMS containing BCPs have been reported to be suitable precursors for ferromagnetic ceramics [21–23]. Poly(dimethylsiloxane)-*b*-PFDMS, poly(methylvinylsiloxane)-*b*-PFDMS, poly(isoprene)-*b*-PFDMS, poly(styrene)-*b*-PFDMS and poly(methyl methacrylate)-*b*-PFDMS were reported to yield rod-like cylindrical micelles in solution [24–26]. Manners and coworkers [27,28] provided evidence that crystallization of the PFDMS core forming block was the driving force for the formation of the cylindrical architectures. The *semi*-crystallinity of the PFDMS-rich core was detected by wide angle X-ray scattering (WAXS) measurements in which peaks with a d spacing of ~6.4 Å were typically observed. The position of the peak was in good agreement with typical spacings reported for *semi*-crystalline PFDMS homopolymer films and PFDMS pentamer single crystals [29,30]. The peak intensity observed was often weak and higher order peaks were typically not detected, suggesting a lower degree of crystallinity of PFDMS in micellar cores compared to PFDMS homopolymer in bulk. Interestingly, results reported by Vancso and coworkers [12] revealed a

* Corresponding author. Tel.: +31 (0) 53 4892967.
E-mail addresses: g.j.vancso@utwente.nl, epj@andoraconsulting.com (G.J. Vancso).
[1] Current address: Universiti Kebangsaan Malaysia, 43600 UKM Bangi, Selangor, Malaysia.

http://dx.doi.org/10.1016/j.polymer.2014.04.021
0032-3861/

rather dynamic PFDMS core for PMMA-*b*-PFDMS micelles assembled in acetone (*i.e.* a selective solvent for PMMA), as was observed with temperature controlled ^{1}H NMR measurements. The absence of a crystalline phase in the PFDMS core for these micelles was independently confirmed by the absence of Bragg peaks in recorded WAXS spectra. These results pointed toward a solvophilicity driven micellar self-assembly process for PMMA-*b*-PFDMS block copolymers in acetone.

While a variety of self-assembled morphologies have been obtained for a range of PFDMS based block copolymers in selective solvents [31–34], reports on their utilization and structural stability on surfaces remain scarce [21]. Wang and coworkers [35] reported on the microfluidic alignment of corona crosslinked poly(-isoprene)-*b*-PFDMS (PI-*b*-PFDMS) cylindrical micelles on flat substrates and their subsequent use as precursors to 1D magnetic ceramic replicas. To our knowledge, there are no accounts of the behavior of non-crosslinked PFDMS-containing micelles on solid substrates in the literature. Such knowledge is of potential interest for utilization in etch resist patterns, guided assembly into ceramic nanolines and fabrication of other functional nanostructures.

This paper describes the melting behavior of platelet-like PI_{76}-*b*-$PFDMS_{76}$ micelles with a *semi*-crystalline core, deposited on either HOPG (hydrophobic) or SiO_2 (hydrophilic) substrates (Fig. 1), as studied by *in situ* temperature controlled AFM. In addition, NanoTA was used as an enabling nanotechnology tool for the thermal analysis of these nanometer sized architectures [36,37] to determine the melting temperature of the crystalline PFDMS phase at the nanoscale. Interestingly, the irreversible formation of a wetting layer upon melting the HOPG supported crystals shed light on the role of interfacial energy between block copolymer based nanostructures and their supporting substrates. Hence, the observed substrate dependent, thermally induced morphology changes provide insight in the molecular organization within PI_{76}-*b*-$PFDMS_{76}$ platelet-like crystals and their thermal transitions.

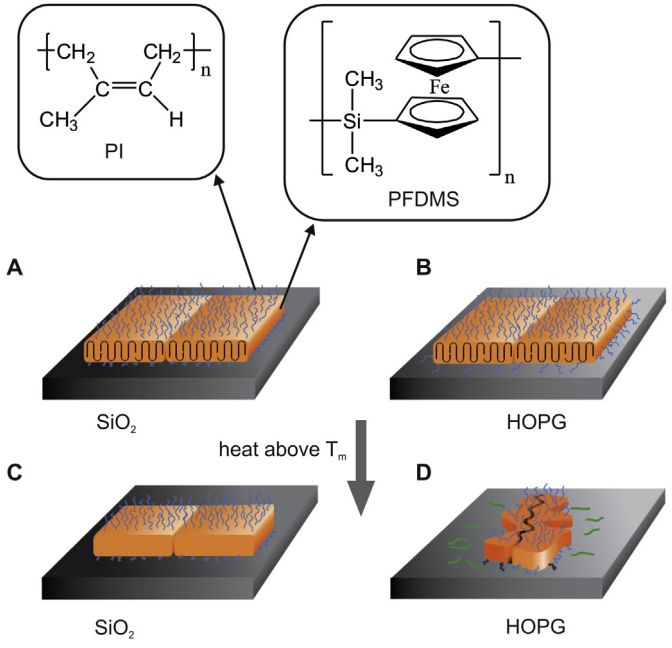

Fig. 1. Schematic representation of PI_{76}-*b*-$PFDMS_{76}$ platelet-like raft crystals deposited on either SiO_2 (A) or HOPG (B) via either spin coating or drop casting. The crystals adopt a platelet-like shape consisting of a crystalline PFDMS core surrounded by a corona of PI (hairy features). Rafts of two or more crystals are frequently observed. The chemical structures of PI and PFDMS are shown in the insets at the left and right top corners, respectively. The horizontal black grating represents the *semi*-crystalline nature of the PFDMS core indicating chain packing order. Upon deposition on SiO_2 or HOPG the crystal shape remains unchanged. Heating above T_m causes the crystals on SiO_2 to shrink in length (C) while on HOPG the crystal morphology disintegrates and small micelle-like architectures (thick black lines) diffuse out of the remainder of the molten crystal (D).

2. Results and discussion

2.1. Deposition of PI_{76}-*b*-$PFDMS_{76}$ crystals at SiO_2

PI_{76}-*b*-$PFDMS_{76}$ platelet-like crystals were formed in *n*-decane and subsequently deposited on either SiO_2 or HOPG by spin-casting. Fig. 2 shows a tapping mode AFM height image of the PI_{76}-*b*-$PFDMS_{76}$ platelet-like crystals (subscript denotes the number average degree of polymerization of each block) at SiO_2 as well as the width, height and length distribution for more than 140 crystals. The height and length of the crystals were determined to be 13.0 ± 1.0 nm and 1.82 ± 0.19 μm, respectively. From Fig. 2B it is obvious that the width distribution has three populations with average crystal widths of 105 ± 14, 201 ± 26 and 285 ± 10 nm.

The nearly double and triple width of the latter two crystals compared to the first crystals indicates that those are not single platelet like crystals, instead they are rafts of two or three adjacent crystals. The black arrows in Fig. 2A point at a primary platelet like crystal (arrow 1) and a raft of two crystals (arrow 2). The high width to height ratios obtained indicate the presence of a core consisting of PFDMS chain folded lamellar domains surrounded by a corona of PI chains. For crystals prepared in another batch the width and height were comparable, yet the length of these crystals was ~4 μm. Furthermore we note that the dimensions of the as casted crystals were similar irrespective whether they were deposited at SiO_2 or HOPG.

XPS spectroscopy was used to obtain information on the composition of the air exposed top layer of the PI_{76}-*b*-$PFDMS_{76}$ crystals deposited at SiO_2 substrates before and after oxygen reactive ion etching (O_2-RIE). The etching step was used to remove organic material from the corona and the core of the crystals in order to expose the iron present in the PFDMS rich core. Fig. 3 shows high resolution XPS Fe2p core spectra of PI_{76}-*b*-$PFDMS_{76}$ platelet-like crystals after deposition on SiO_2 substrates before and after O_2-RIE. Before plasma etching no Fe was detected, indicating that the PFDMS rich core is indeed fully covered by a PI corona of at least 7 nm thick (*i.e.* the estimated escape depth of the photoelectrons for the used take-off angle of 45°). Following plasma etching, in which the organic material was removed, Fe2p bands at 712.7 eV (2p3/2) and 726.1 eV (2p1/2) were observed. These bands are ascribed to the presence of Fe in a higher oxidation state (due to O_2-RIE) compared to Fe in ferrocene [38].

2.2. Nanoscale thermal analysis of PI_{76}-*b*-$PFDMS_{76}$ crystals

NanoTA was used to determine the melting transition temperature of PI_{76}-*b*-$PFDMS_{76}$ platelet-like crystals deposited on SiO_2 surfaces. NanoTA is an emerging nanotechnology tool that exploits heatable AFM probes for the spatially controlled thermal analysis of soft matter. Typically the deflection of the AFM cantilever is monitored as a function of the calibrated probe tip temperature in constant height AFM imaging mode [37]. Upon increasing the tip temperature, the sample area in close proximity to the tip contact point is heated. Hence the sample will thermally expand, which is measured as an increase in cantilever deflection. Once the melting temperature of a sample is reached, the material softens and the tip starts to penetrate into the sample surface. This is monitored as a marked decrease in the deflection signal. Despite several attempts on individual PI_{76}-*b*-$PFDMS_{76}$ platelet-like crystals, no transition temperature was detected by NanoTA. This is explained by *i*) the crystal geometry, *i.e.* the crystals are very thin and as a consequence

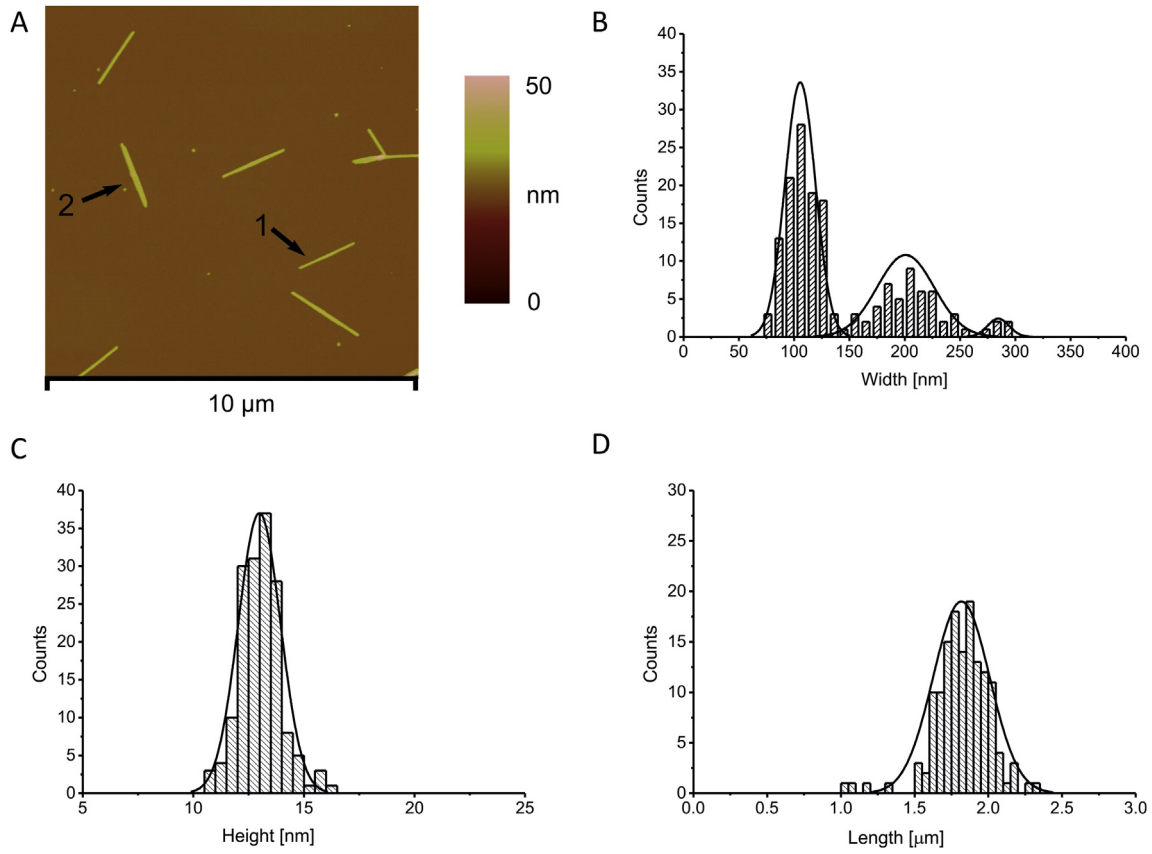

Fig. 2. Tapping mode AFM height image of PI_{76}-*b*-$PFDMS_{76}$ crystals deposited on SiO_2 (A) and the width (B), height (C) and length (D) distribution of these as casted crystals ($n > 140$).

the small penetration of the heated probe tip into the crystal upon melting of the PFDMS core is not detectable and *ii*) the presence of silicon (good thermal conductor) close to the tip–sample interface cools down the probe tip significantly on these thin structures [38]. Hence the probe tip temperature is assumed to significantly deviate from the previously calibrated "set" temperature. In other words, thermal analysis of single PI_{76}-*b*-$PFDMS_{76}$ platelet-like crystals appears to exceed the physical limits of the technique.

Drop casting of PI_{76}-*b*-$PFDMS_{76}$ crystals onto SiO_2 resulted in the formation of stacked crystal layers with micrometer thicknesses. NanoTA runs on these aggregates were successful. Fig. 4 shows a NanoTA graph of the crystals in which the probe tip temperature was ramped from 50 °C up to 200 °C at 10 °C s^{-1}. Since the PI corona continues to expand even upon melting of the PFDMS core, a marked drop typically observed for crystalline homopolymers is absent. Instead a lower overall thermal expansion is observed. The apparent melting point ($T_{m,app}$) is now defined as the intersect of the slopes at which both PI and PFDMS thermally expand and the horizontal plateau in which thermal expansion (PI) and sample penetration (molten PFDMS) are balanced. A value of 122 ± 10 °C was obtained for $T_{m,app}$. This value is in good agreement with the melting temperature determined by DSC measurements on bulk PI_{76}-*b*-$PFDMS_{76}$ samples (see Supporting Information). The relatively large error of ±10 °C is ascribed to the use of polymers as melting point standards for the probe tip temperature calibration in NanoTA [39].

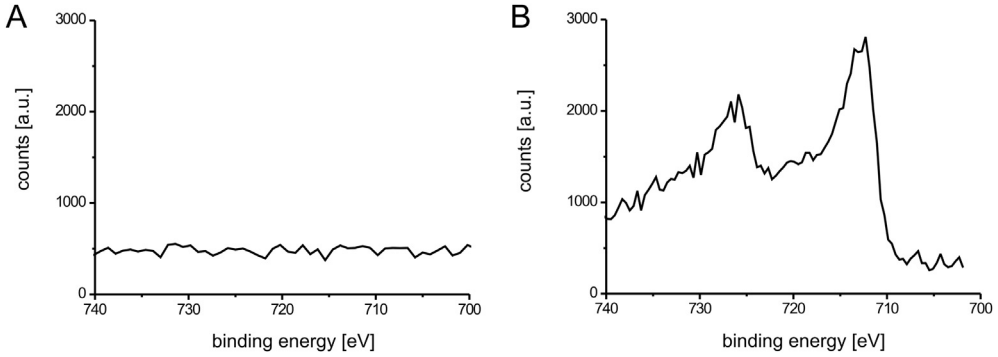

Fig. 3. High resolution XPS Fe2p core spectra of PI_{76}-*b*-$PFDMS_{76}$ crystals deposited on silicon substrates before (A) and after (B) O_2-RIE. Before etching no Fe was detected while upon etching the Fe rich PFDMS core was revealed, indicating that the PFDMS core was fully covered by a PI corona.

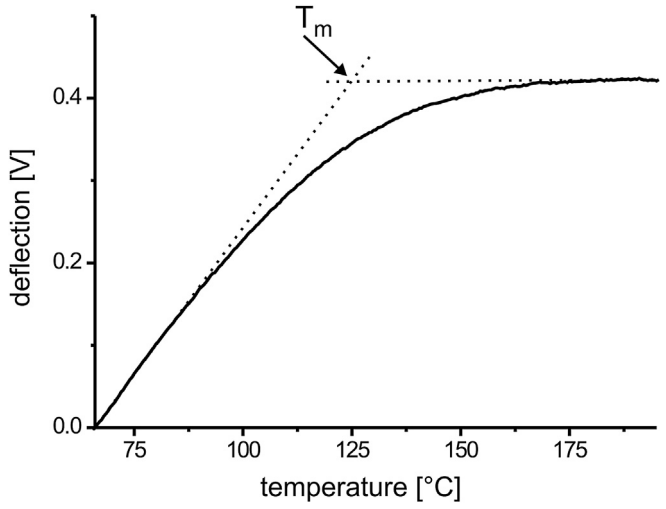

Fig. 4. NanoTA graph of PI_{76}-*b*-$PFDMS_{76}$ crystals drop casted on SiO_2. The apparent melting point was calculated to be 122 ± 10 °C (intercept of the two dotted lines). The temperature was ramped at 10 °C s^{-1}.

2.3. Isothermal AFM of PI_{76}-*b*-$PFDMS_{76}$ crystals at elevated temperatures

Fig. 5 shows temperature controlled tapping mode AFM height images of PI_{76}-*b*-$PFDMS_{76}$ platelet-like crystals deposited on SiO_2. The images shown were captured subsequently at room temperature, 80 °C, 100 °C and 130 °C and are part of a series following a temperature ramp profile mentioned in the figure caption. The most obvious change observed in crystal dimensions is the decrease in crystal length with increasing temperature, starting from 80 °C and above. This decrease in crystal length occurred during the first few minutes after a temperature increase. Heating to 130 °C typically resulted in a 17 ± 3% decrease in length. Upon increasing the temperature with several degrees, the AFM is needed to equilibrate for a few minutes in order to eliminate thermal drift during subsequent imaging. Identifying the same crystals is required a few minutes as well. Hence, AFM images were typically collected 20 min after increasing (or decreasing) the temperature. Unfortunately this limited temporal resolution did not allow us to obtain any kinetic information on the observed decrease in crystal length. Prolonged heating (up to 3 h) of the crystals at the set temperatures resulted in little or no further decrease in length. At temperatures up to 160 °C the crystals retained their platelet-like shape. Upon cooling to room temperature it was observed that the decrease in length was irreversible.

Fig. 6 shows temperature controlled tapping mode AFM phase images of PI_{76}-*b*-$PFDMS_{76}$ platelet-like crystals deposited on HOPG recorded at temperatures from room temperature up to 120 °C for different heating times. In Fig. 6 the platelet crystal rafts are clearly resolved. Interestingly the crystals showed a slight decrease in length at temperatures above 100 °C, with the formation of a very thin wetting layer surrounding the crystals (see Fig. 6E), which contrasts with the observed changes for the crystals deposited on SiO_2. The thickness of this layer was estimated from the corresponding AFM height images to be below 1 nm. This thin wetting layer is likely formed by diffusion of PI-*b*-PFDMS molecules from the crystals to the HOPG surface. This observation is in agreement with the practical and theoretical work of Riegler and Köhler [40], which describes the partial melting of a solid deposited on a surface at temperatures below its melting point if the respective liquid wets the adjoining interface. Due to the limited temporal resolution of the *in situ* temperature controlled AFM measurements the fast dynamics of the formation of the wetting layer at 100 °C could not be resolved. At 120 °C the crystals show a typical molten morphology and this transition temperature is in good agreement with the melting temperatures measured by DSC (bulk, see Supporting Information) and NanoTA.

Control experiments with freshly cleaved HOPG surfaces without deposited crystals, following an identical temperature profile, did not reveal the presence of surface attached material originating from the environment that could explain the presence of a wetting layer on HOPG at elevated temperatures. In addition, the same temperature profile was used to heat crystals that possessed a cross-linked PI shell deposited on SiO_2 and HOPG surfaces. In this case, the formation of a polymeric wetting layer was not observed during the respective temperature controlled AFM measurements (see Supporting Information). To evaluate whether iron originating from PFDMS became exposed to the surface after melting, XPS measurements were performed on non cross-linked crystals deposited on SiO_2 and HOPG surfaces, before and after heating at 130 °C for 3 h. No iron was detected for crystals deposited on SiO_2 surfaces before and after melting. This is in agreement with the observation that the crystals deposited retained their platelet-like shape. For crystals deposited on HOPG, no iron was detected with XPS, while for the respective molten crystals Fe2p peaks were clearly observed at 708.8 eV (2p3/2) and 721.5 eV (2p1/2). These Fe2p peak positions are in good agreement with values reported earlier for Fe in ferrocene [41] and PFDMS homopolymers, respectively [20]. These results indicate the presence of PFDMS in the wetting layer observed on HOPG after heating of the crystals.

This remarkable difference in behavior of the crystals on SiO_2 and HOPG upon increasing the temperature is explained in terms of the substrate wettability by PI and PFDMS, respectively [42]. As the platelet-like crystals melt, the PI corona chains are no longer anchored at the PI_{76}-*b*-$PFDMS_{76}$ interface and acquire increased mobility. Consequently PI starts to wet the HOPG surface which is observed as the diffusion of the small PI_{76}-*b*-$PFDMS_{76}$ aggregates in Fig. 6D–F (in Fig. 6E the white arrows point toward two of these aggregates).

As a control experiment thiol end-capped $PFDMS_{64}$ was used to obtain $PFDMS_{64}$ homopolymer platelet-like crystals on HOPG surfaces and their thermal behavior was studied. Fig. 7 shows tapping mode AFM images of the $PFDMS_{64}$ homopolymer platelet-like crystals on HOPG at room temperature and after being exposed *ex situ* to 150 °C for 30 min. The heating temperature was above the melting point of the $PFDMS_{64}$ bulk polymer. It is obvious from Fig. 7 that the platelet-like structure remains intact even after heating the crystals above the melting temperature. This is in agreement with the explained differences in wetting behavior of the PI_{76}-*b*-$PFDMS_{76}$ platelet like crystals. In addition, contact angle measurements of PI and quenched PFDMS melts on SiO_2 and HOPG surfaces showed a preferred wetting (spreading) of PI on HOPG whereas on SiO_2 no preferred wetting was observed. These measurements are in agreement with results reported by Butt and coworkers [43] and by Vancso and coworkers [44].

In some rare cases for PI_{76}-*b*-$PFDMS_{76}$ crystals deposited on SiO_2, especially when two crystals were stacked on top of each other, crystal thickening was observed for temperatures around 130 °C. Fig. 8 shows a temperature controlled tapping mode AFM height image as an example. The observed effect is ascribed to lamellar thickening. In analogy to DSC measurements (see Supporting Information) of the bulk PI_{76}-*b*-$PFDMS_{76}$ material, this might be explained by recrystallization of type I lamella at

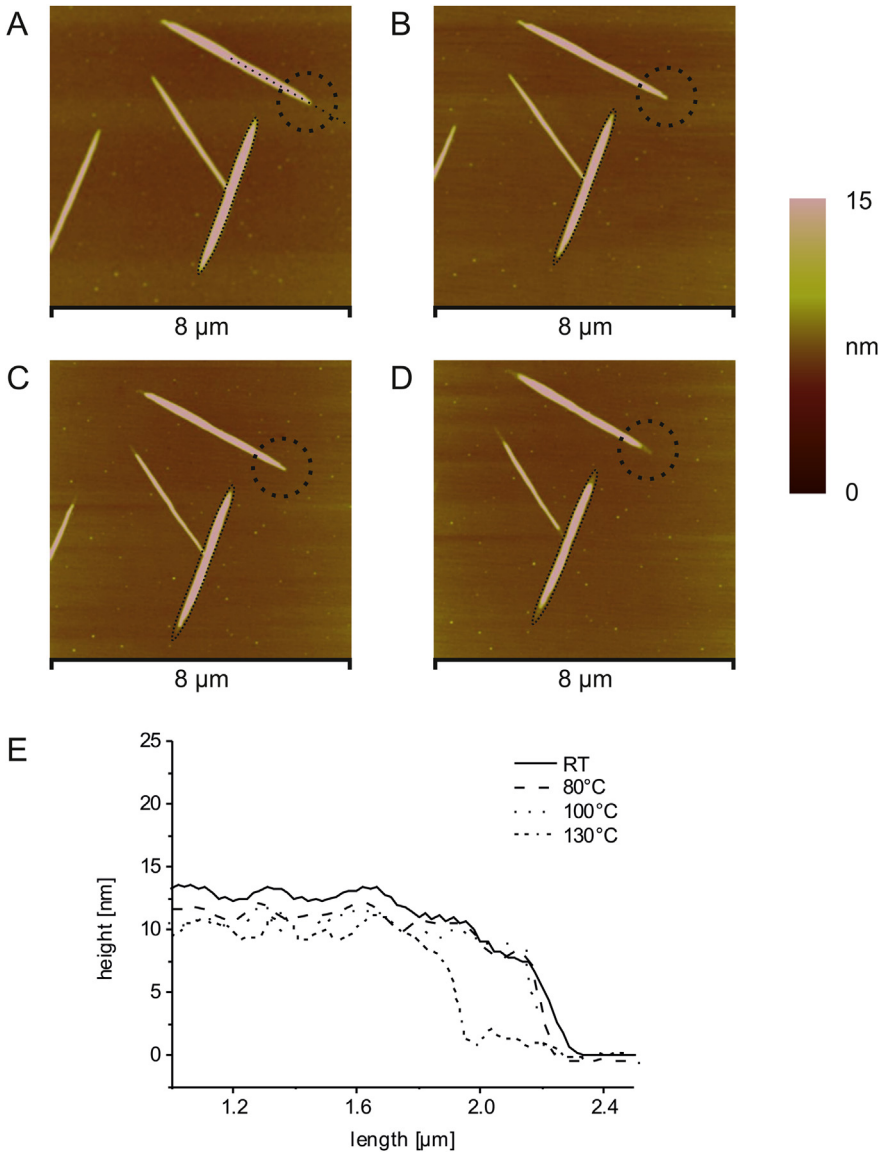

Fig. 5. Temperature controlled tapping mode AFM height images of platelet-like PI_{76}-*b*-$PFDMS_{76}$ crystals on SiO_2. The images shown here are recorded at room temperature (A), after 20 min at 80 °C (B), after 20 min at 100 °C (C) and after 20 min at 130 °C (D), respectively. The decrease in length upon increasing the temperature above 80 °C is obvious when examining the crystal end located in the black dotted circles as well as from the overlay of the contour (thin dotted line) of one crystal at room temperature (A) on the same crystal at higher temperatures (B–D). The corresponding cross-sections along the upper crystal longitudinal axis represented by the black dotted line in A are shown in E. Note: the *z* scale (A–D) was saturated for reasons of clarification. The followed temperature program started at room temperature followed by subsequent heating for 80 min at 80 °C, 30 min at 100 °C, 150 min at 120 °C and finally 130 min at 130 °C.

temperatures above 120 °C to form thicker type II lamella that have a higher melting point. After prolonged heating at increased temperatures (up to 160 °C, images not shown) the well-defined shape of the crystals remained. However, the arms of the crossed crystals decreased in length, accompanied by an increase in height, which is indicative of lamellar thickening. Clearly, molecular rearrangements occurred in the melt in order to minimize the free energy of the structure.

Despite the interesting phenomena observed upon heating PI_{76}-*b*-$PFDMS_{76}$ crystals on SiO_2 and HOPG substrates, many fundamental questions remain open. The possible explanations provided in the discussion must be investigated in depth by using for example, electron diffraction measurements in order to provide detailed insight in the crystallinity of the samples at different temperatures. However here it was clearly shown that substrate interfacial energy strongly influences the morphology of PI_{76}-*b*-$PFDMS_{76}$ crystals deposited on substrates as temperature is increased.

3. Conclusions

The self-assembly of PI_{76}-*b*-$PFDMS_{76}$ in a PI selective solvent is a crystallization driven process resulting in the formation of platelet-like crystals with a *semi*-crystalline PFDMS core and solvent swollen PI corona. AFM analysis of these crystals, deposited on either SiO_2 or HOPG, showed that height and width of these crystals were nearly identical after drying and that rafts of two or more crystals exist. XPS analysis of PI_{76}-*b*-$PFDMS_{76}$ crystals deposited on SiO_2 before and after O_2-RIE confirmed the presence of a PI corona around a PFDMS core. The apparent melting temperature of the *semi*-crystalline PFDMS core was determined with NanoTA to be 122 ± 10 °C. *In situ* examination of PI_{76}-*b*-$PFDMS_{76}$ crystals

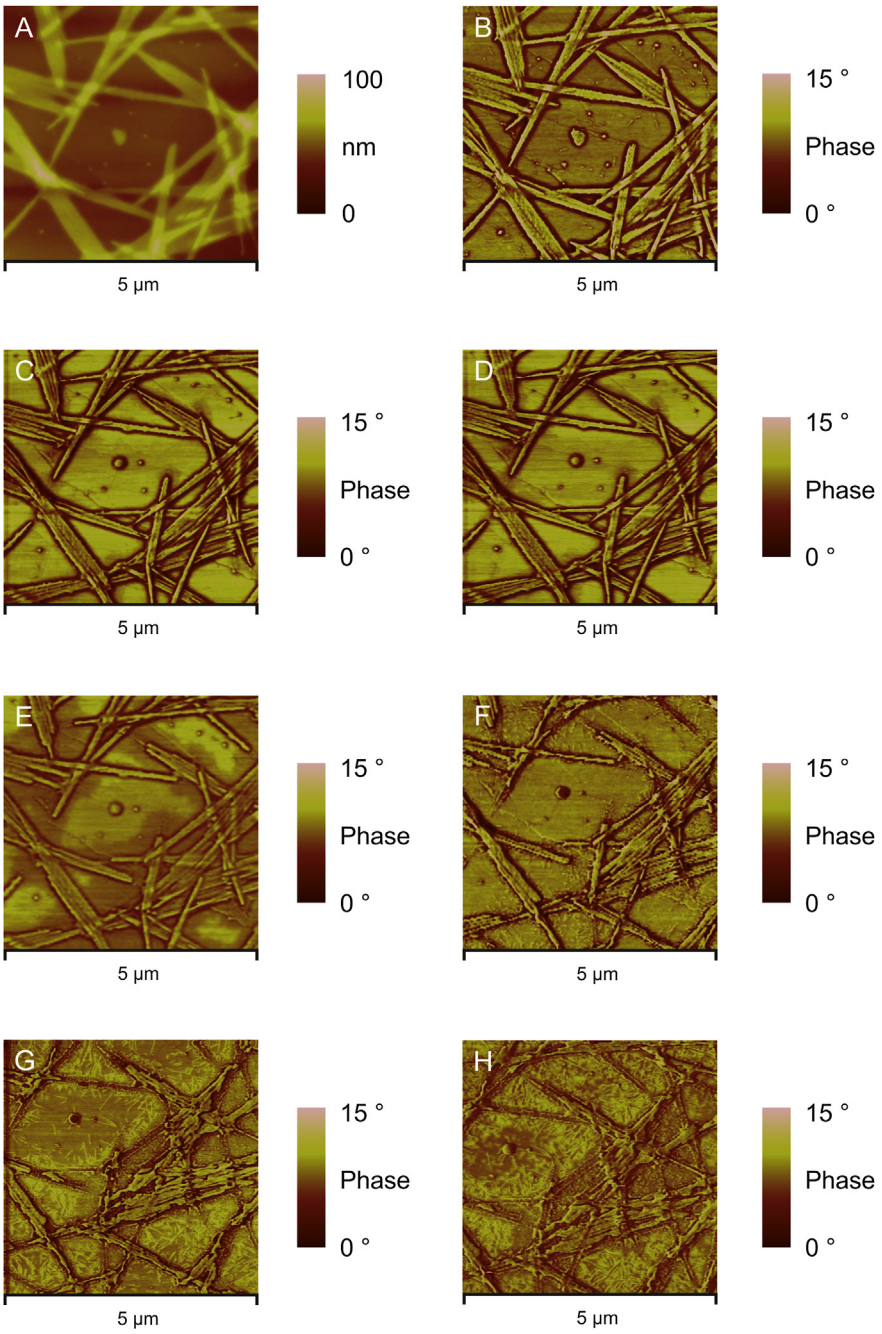

Fig. 6. A series of AFM height (A) and phase (B–H) images of PI_{76}-*b*-$PFDMS_{76}$ crystals on HOPG collected with temperature controlled tapping mode AFM at (A) and (B) room temperature, (C) and (D) 80 °C (images collected after 60 min and 85 min), (E) 100 °C (formation of HOPG wetting layer can be observed) and (F)–(H) 120 °C (images collected after 30 min, 185 min and 490 min), respectively.

deposited on SiO_2 or HOPG with temperature controlled AFM revealed that on SiO_2 the crystals irreversibly decreased their length when heated above their expected melting temperature, whereas on HOPG the crystals showed a decrease in length upon heating below their expected melting temperature, while when heated above this temperature a typical morphology characteristic for molten layers and the irreversible formation of a thin wetting layer was observed. The observed differences in morphology of PI_{76}-*b*-$PFDMS_{76}$ crystals deposited on SiO_2 and HOPG as temperature was increased emphasize that the interfacial energy between polymer based assemblies and supporting substrates governs the stability of these self-assembled nanostructures.

4. Experimental

4.1. Materials

The PI_{76}-*b*-$PFDMS_{76}$ diblock copolymer with a narrow molar mass distribution was synthesized by sequential living anionic polymerization in THF as described elsewhere [27,45,46]. PI-*b*-PFDMS platelet-like crystals were prepared by dissolving 2.2 mg PI_{76}-*b*-$PFDMS_{76}$ in a mixture of *n*-decane (20 mL) and xylene (2 mL) in a vial (50 mL) thermostated at 100 °C (oil bath). Following complete dissolution of the block copolymer, the temperature was lowered to 70 °C and kept for 12 h. Subsequently the oil bath was

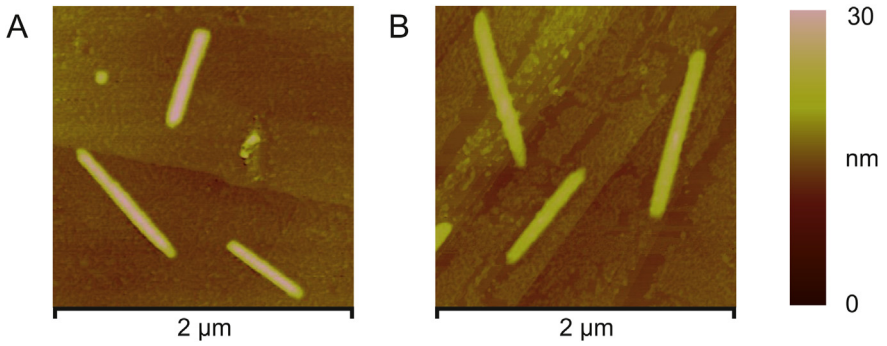

Fig. 7. Tapping mode AFM height images of thiol end-capped $PFDMS_{64}$ homopolymer crystals grown from solution on HOPG at room temperature (A) and after being exposed *ex situ* to 150 °C for 30 min (B).

cooled to room temperature in 2 to 3 h. The samples were stored in solution at room temperature. The solutions were used within two days. Prior to deposition the solution was agitated by hand shaking for 1 min. PI_{76}-*b*-$PFDMS_{76}$ crystals were deposited on 1 cm × 1 cm silicon (CZ, type P, Boron, ⟨100⟩, diameter 100 mm, OKMETIC, Vantaa, Finland) or freshly cleaved HOPG (Agar Scientific Limited, Stansted, United Kingdom) substrates via drop casting or spin coating (1500 rpm, 30 s, Suss MicroTec Delta20 spincoater, Garching/Hochbrück, Germany) a 0.5 mL aliquot of the crystal solution. The samples were allowed to dry in air followed by drying in vacuum at 60 °C for 12 h.

Thiol end-capped $PFDMS_{64}$ homopolymer with a narrow molar mass distribution was synthesized by sequential living anionic polymerization in THF as described elsewhere [47]. A freshly cleaved HOPG surface was immersed in a 1 mg/mL degassed toluene solution of $PFDMS_{64}$ for 24 h, to form the platelet-like

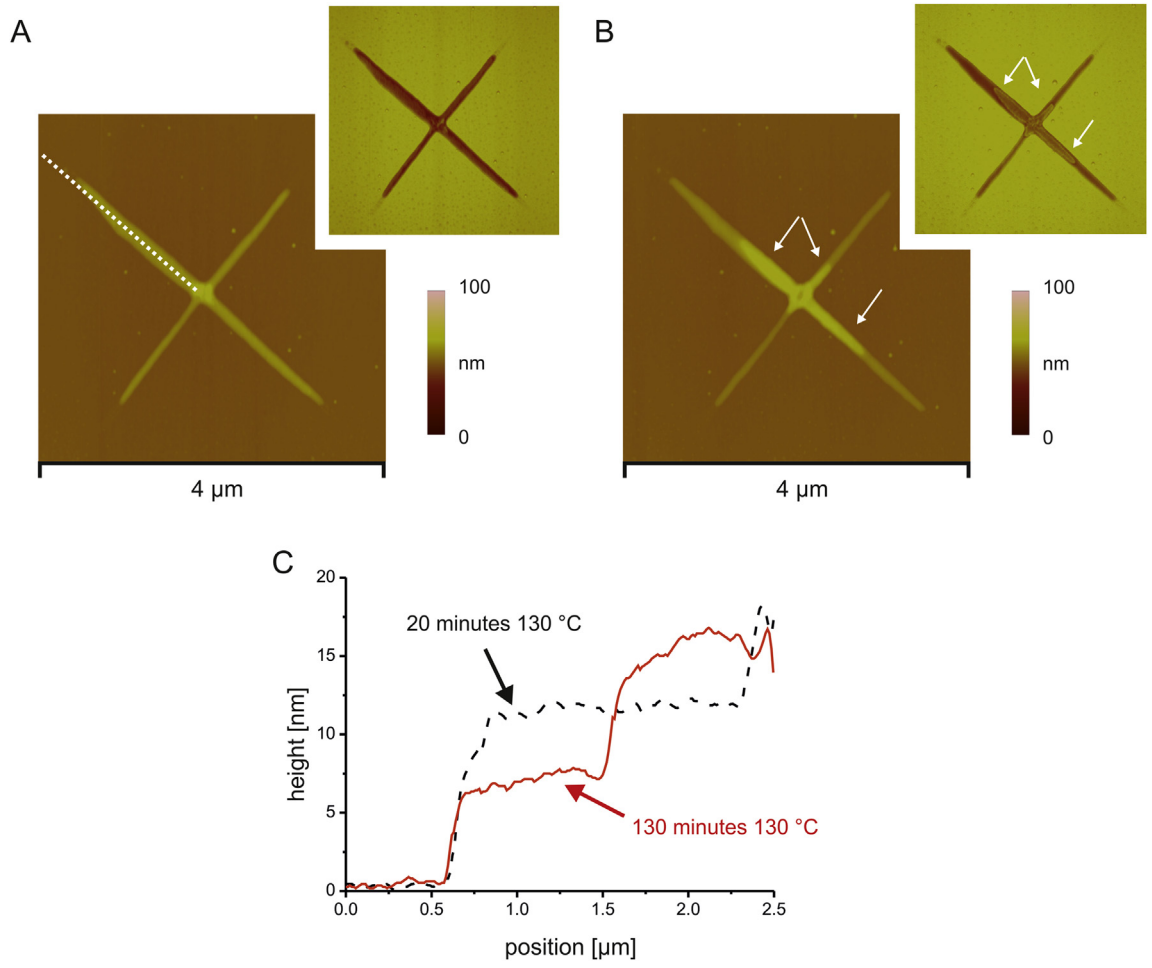

Fig. 8. Tapping mode AFM height images of PI_{76}-*b*-$PFDMS_{76}$ crystals on SiO_2 at 130 °C for 20 min (A) and 130 °C for 130 min (B) showing the growth of a thickened layer upon prolonged heating at 130 °C (marked by the white arrows in B). The insets in A and B are corresponding tapping mode AFM phase images (*z* scale 120°). The corresponding cross-sections along the crystal longitudinal axis represented by the white dotted line in A are shown in (C).

homopolymer PFDMS crystals on the surface. Subsequently, the substrate was washed by immersing into toluene and dichloromethane for 10 min each followed by drying under a N_2 stream. For the temperature treatment the HOPG substrate was placed into a preheated oven at 150 °C for 30 min in air atmosphere.

Silicon surfaces were extensively rinsed with toluene and ethanol and dried under a nitrogen stream prior to use. HOPG substrates were freshly cleaved prior to use.

4.2. Temperature controlled AFM

The thermal behavior of the PI_{76}-*b*-$PFDMS_{76}$ platelet-like crystals on silicon or HOPG supports was studied with a Multimode Nanoscope IIIa (Bruker/Veeco Santa Barbara, CA, USA) AFM equipped with a Digital Instruments Multimode Heater/Cooler accessory (Bruker/Veeco, Santa Barbara, CA, USA). The latter primarily consists of a sample heater and a probe holder with integrated cantilever heater. During the experiments the sample heater and probe holder were set to the same temperatures. The AFM was operated in tapping mode using silicon cantilevers with a resonance frequency and spring constant of ~330 kHz and ~42 N m^{-1}, respectively (PPP-NCH-W, Nanosensors, Wetzlar, Germany). Images under ambient conditions were taken at temperatures ranging from room temperature up to 160 °C after 10 min of thermal equilibration.

4.3. Nanoscale thermal analysis

Heatable AFM probes (type AN-2, with 200 μm long cantilevers, Anasys Instruments, Santa Barbara, CA, USA) mounted in a Dimension D3100 equipped with a hybrid 153 scanner and a NanoScope IVa controller (Bruker/Veeco, Santa Barbara, CA, USA) were used for the highly localized nanoscale thermal analysis of drop casted PI_{76}-*b*-$PFDMS_{76}$ crystals on silicon. The probe temperature was controlled with a Nano-TA2 controller (Anasys Instruments, Santa Barbara, CA, USA). The temperature was ramped from 60 °C to 240 °C at 10 °C s^{-1}. Prior to the experiments the probe temperature was calibrated using polymer standards with known melting points: poly(ε-caprolactone) (PCL, T_m = 55 °C), poly(ethylene) (PE, T_m = 116 °C) and poly(ethylene terephthalate) (PET, T_m = 235 °C).

4.4. Differential scanning calorimetry (DSC)

Bulk PI_{76}-*b*-$PFDMS_{76}$ samples of about 5 mg were placed in a Perkin–Elmer DSC-7 (Waltham, MA, USA). After erasing the thermal history of the sample at 150 °C for 5 min, the samples were isothermally crystallized at T_c (between 80 °C up to 110 °C) for 120 min. The melt was cooled to T_c at 200 °C min^{-1}. From T_c the sample was heated at 10 °C min^{-1} to 150 °C in order to observe the melting transition.

4.5. O_2-RIE

PI_{76}-*b*-$PFDMS_{76}$ crystals on silicon were exposed to oxygen plasma in a reactive ion etch (O_2-RIE) setup (Elektrotech PF340, London, United Kingdom) for 30 s. The setup was operated at 50 W, 10 mTorr and 20% O_2.

4.6. X-ray photoelectron spectroscopy

XPS spectra of untreated and heated PI_{76}-*b*-$PFDMS_{76}$ crystals deposited on SiO_2 and HOPG as well as of plasma etched PI_{76}-*b*-$PFDMS_{76}$ crystals on SiO_2 were recorded on a PHI Quantera XPS microprobe (Physical Electronics Inc., Chanhassen, MN, USA) using a monochromatic X-ray beam (Al Kα monochromatic at 1486.6 eV, 100 μm diameter, 25 W) at a fixed take-off angle of 45° (φ) immediately after sample preparation. Charging of samples was corrected by shifting the peak positions relative to the position of neutral carbon at 285.0 eV (C1s). Atomic concentrations were determined by numerical integration of the relative peak areas using Multipak software with supplied atomic sensitivity factors relative to F1s (C1s: 0.314; O1s: 0.733; Si2p: 0.368; Fe2p: 2.946) [48].

4.7. Contact angle measurements

Static contact angles of PI and quenched melts of PFDMS on SiO_2 and HOPG were measured with a CA microscope (Data Physics OCA model 15 Plus, Filderstadt, Germany) at room temperature. PFDMS samples were molten at 165 °C for 5 min and quenched to room temperature. PI was not additionally heated. Data for three different spots for each substrate were averaged.

Acknowledgment

This work was supported by NanoImpuls/NanoNed, the nanotechnology program of the Dutch Ministry of Economic Affairs (Grant TPC.6940), by NanoNextNL, a micro and nanotechnology consortium of the Government of the Netherlands and 130 partners, by the NWO TOP Grant 700.56.322 and by the NWO Middelgroot Grant 700.54.102.

Appendix A. Supplementary material

Supplementary data related to this article can be found at http://dx.doi.org/10.1016/j.polymer.2014.04.021.

References

[1] Kim Y, Dalhaimer P, Christian DA, Discher DE. Nanotechnology 2005;16:S484.
[2] Jo YS, van der Vlies AJ, Gantz J, Thacher TN, Antonijevic S, Cavadini S, et al. J Am Chem Soc 2009;131:14413.
[3] Lee Y, Ishii T, Kim HJ, Nishiyama N, Hayakawa Y, Itaka K, et al. Angew Chem Int Ed Engl 2010;49:2552.
[4] Quan CY, Chen JX, Wang HY, Li C, Chang C, Zhang XZ, et al. ACS Nano 2010;4:4211.
[5] Ge J, Lu D, Liu Z, Liu Z. Biochem Eng J 2009;44:53.
[6] Mai Y, Eisenberg A. J Am Chem Soc 2010;132:10078.
[7] Chen Q, Schönherr H, Vancso GJ. Small 2009;5:1436.
[8] Cui C, Bonder EM, Jäkle F. J Am Chem Soc 2010;132:1810.
[9] Glass R, Möller M, Spatz JP. Nanotechnology 2003;14:1153.
[10] Bansmann J, Kielbassa S, Hoster H, Weigl F, Boyen HG, Wiedwald U, et al. Langmuir: ACS J Surf Colloids 2007;23:10150.
[11] Hu Y, Chen D, Park S, Emrick T, Russell TP. Adv Mater 2010;22:2583.
[12] Korczagin I, Hempenius MA, Fokkink RG, Cohen Stuart MA, Al-Hussein M, Bomans PHH, et al. Macromolecules 2006;39:2306.
[13] Kulbaba K, Manners I. Macromol Rapid Commun 2001;22:711.
[14] Shen L, Wang H, Guerin G, Wu C, Manners I, Winnik MA. Macromolecules 2008;41:4380.
[15] Qian J, Zhang M, Manners I, Winnik MA. Trends Biotechnol 2010;28:84.
[16] Hempenius MA, Cirmi C, Song J, Vancso GJ. Macromolecules 2009;42:2324.
[17] Shi WQ, Giannotti MI, Zhang XZ, Hempenius MA, Schönherr H, Vancso GJ. Angew Chem Int Ed 2007;46:8400.
[18] Wang H, Wang XS, Winnik MA, Manners I. J Am Chem Soc 2008;130:12921.
[19] Acikgoz C, Ling XY, Phang IY, Hempenius MA, Reinhoudt DN, Huskens J, et al. Adv Mater 2009;21:2064.
[20] Lammertink RGH, Hempenius MA, Chan VZH, Thomas EL, Vancso GJ. Chem Mater 2001;13:429.
[21] Cao L, Massey JA, Winnik MA, Manners I, Riethmüller S, Banhart F, et al. Adv Funct Mater 2003;13:271.
[22] Massey JA, Winnik MA, Manners I, Chan VZH, Ostermann JM, Enchelmaier R, et al. J Am Chem Soc 2001;123:3147.
[23] Wang XS, Ozin GA, Winnik MA, Manners I. J Am Chem Soc 2003;125:12686.
[24] Korczagin I, Hempenius MA, Vancso GJ. Macromolecules 2004;37:1686.
[25] Rider DA, Manners I. Polym Rev 2007;47:165.
[26] Manners I. Chem Commun; 1999:857.
[27] Massey JA, Temple K, Cao L, Rharbi Y, Raez J, Winnik MA, et al. J Am Chem Soc 2000;122:11577.

[28] Raez J, Manners I, Winnik MA. J Am Chem Soc 2002;124:10381.
[29] Rasburn J, Petersen R, Jahr T, Rulkens R, Manners I, Vancso GJ. Chem Mater 1995;7:871.
[30] Rulkens R, Lought AJ, Manners I, Lovelance SR, Grant C, Geiger WE. J Am Chem Soc 1996;118:12683.
[31] Qian J, Guerin G, Lu Y, Cambridge G, Manners I, Winnik MA. Angew Chem Int Ed 2011;50:1622.
[32] Qian J, Lu Y, Cambridge G, Guerin G, Manners I, Winnik MA. Macromolecules 2012;45:8363.
[33] Rupar PA, Chabanne L, Winnik MA, Manners I. Science 2012;337:559.
[34] Qian J, Lu Y, Chia A, Zhang M, Rupar PA, Gunari N, et al. ACS Nano 2013;7.
[35] Wang XS, Liu K, Arsenault C, Rider DA, Ozin GA, Winnik MA, et al. J Am Chem Soc 2007;129:5630.
[36] Duvigneau J, Schönherr H, Vancso GJ. ACS Nano 2010;4:6932.
[37] Nelson BA, King WP. Rev Sci Instrum; 2007:023702.
[38] Zhou J, Berry B, Douglas JF, Karim A, Snyder CR, Soles C. Nanotechnology 2008;19:495703.
[39] Nelson BA, King WP. Sensors Actuat Phys 2007;140:51.
[40] Riegler H, Köhler R. Nat Phys 2007;3:890.
[41] Briggs D, Seah MP. Practical surface analysis: by Auger and X-ray photoelectron spectroscopy. Chichester, UK: Wiley; 1983.
[42] Magonov SN, Yerina NA, Godovsky YK, Reneker DH. J Macromol Sci Part B: Phys 2006;45:169.
[43] Stark R, Bonaccurso E, Kappl M, Butt HJ. Polymer 2006;47:7259.
[44] Roerdink M, Hempenius MA, Gunst U, Arlinghaus HF, Vancso GJ. Small 2007;3:1415.
[45] Ni YZ, Rulkens R, Manners I. J Am Chem Soc 1996;118:4102.
[46] Gädt T, Ieong NS, Cambridge G, Winnik MA, Manners I. Nat Mater 2009;8:144.
[47] Peter M, Lammertink RGH, Hempenius MA, Vancso GJ, van Os M, Knoll W, et al. Chem Commun 1999;1:359.
[48] Zhao J, Garza EG, Lam K, Jones CM. Appl Surf Sci 2000;158:246.